Article

Recent Strengthening of the ENSO Influence on the Early Winter East Atlantic Pattern

Jiayi Hou [1,2], Zheng Fang [1,2] and Xin Geng [1,2,3,*]

1   CIC-FEMD/ILCEC, Key Laboratory of Meteorological Disaster of Ministry of Education (KLME), Nanjing University of Information Science and Technology, Nanjing 210044, China
2   School of Atmospheric Science, Nanjing University of Information Science and Technology, Nanjing 210044, China
3   Division of Environmental Science and Engineering, Pohang University of Science and Technology, Pohang 37673, Republic of Korea
*   Correspondence: gengxin@nuist.edu.cn

Abstract: Previous studies have demonstrated that the influence of the El Niño–Southern Oscillation (ENSO) on the Euro-Atlantic atmospheric circulation varies considerably during the boreal winter. Compared to the late winter (January–March) relationship, the early winter (November–December) teleconnection is more uncertain and less understood. In this paper, we revisited this early winter regional ENSO teleconnection using the Hadley Centre Global Sea Ice and Sea Surface Temperature (HadISST) and the European Centre for Medium-Range Weather Forecasting (ECMWF) fifth generation reanalysis (ERA5) datasets for the period 1979–2022. It was found that the signal projected well onto the second dominant mode of Euro-Atlantic atmospheric variability, the East Atlantic Pattern (EAP), rather than the previously mentioned North Atlantic Oscillation (NAO). This influence is associated with ENSO-induced dipolar convection anomalies in the Gulf of Mexico and Caribbean Sea (GMCA), which leads to an EAP via exciting Rossby waves propagating northward into the North Atlantic. We further revealed that this ENSO–EAP teleconnection underwent a pronounced interdecadal strengthening around the late 1990s. Prior to the late 1990s, the convective response to ENSO in the GMCA was weak. The atmospheric responses over the Euro-Atlantic were mainly driven by the ENSO-induced convective forcing in the tropical Indian Ocean, which favors an NAO-like pattern. In contrast, since the late 1990s, ENSO has induced stronger precipitation anomalies in the GMCA, which exert a dominant influence on the Euro-Atlantic atmospheric circulation and produce an EAP. These results have useful implications for the further understanding of ENSO-related early winter atmospheric and climate variability in the Euro-Atlantic region.

Keywords: ENSO; East Atlantic Pattern; North Atlantic Oscillation; ENSO teleconnection; early winter

1. Introduction

The climate impacts of the El Niño–Southern Oscillation (ENSO) have been demonstrated almost everywhere on the globe [1–3], including remote areas outside the Pacific, such as the Euro-Atlantic sector [4]. The canonical atmospheric response over this region is first detected in the boreal late winter (January–March) and resembles a negative (positive) phase of the North Atlantic Oscillation (NAO) during El Niño (La Niña) conditions [4]. However, unlike the climate response in the North Pacific and North America, which is relatively robust and well understood, the ENSO effect in this region is subject to considerable uncertainty [5–7].

It is demonstrated that the Euro-Atlantic ENSO signal varies nonlinearly with ENSO strength [8–10], is sensitive to ENSO flavors [11,12], and exhibits robust subseasonal nonstationarity from November to March [13–15]. During the early winter (November–December) of El Niño events, the Euro-Atlantic atmospheric response is characterized by a negative

sea level pressure (SLP) anomaly in the midlatitudes and a positive anomaly in the subtropics [14–17]. But the response abruptly reverses its sign in early January [18], and a negative NAO pattern is present thereafter [15,19,20]. The mechanisms responsible for the ENSO teleconnection also differ between early and late winter. While the former is mostly due to the Rossby waves excited by the ENSO-induced tropical convection anomalies [14,15,17], the latter is generally considered as a consequence of a combination of ENSO-related tropical North Atlantic sea surface temperature (SST) modulation [21,22], tropospheric Rossby waves or transient eddies [20,23], and stratospheric processes involving a perturbed polar vortex [19,24,25]. Although ENSO can be satisfactorily predicted by the models in dynamical prediction systems [26,27], the spatio-temporal complexity of this ENSO teleconnection has posed a major challenge for climate models to skillfully capture the Euro-Atlantic wintertime atmospheric circulation anomalies associated with ENSO [6].

The low fidelity of the ENSO influence on the Euro-Atlantic climate in global climate models is suggested to be more severe in early winter than that in late winter [28,29], indicating a need for further understanding. Although the model biases of the ENSO SST or convection feature may be one of the reasons [14], we would like to point out here that even for observations, the climate research community has not reached a consensus on the question about what the ENSO influence on the early winter Euro-Atlantic atmospheric circulation is and how this influence is generated. While some studies claim an ENSO–NAO teleconnection in early winter [15,17], other studies suggested that the ENSO signal corresponds to an East Atlantic pattern (EAP) [30,31]. As we know, the NAO and the EAP are two dominant modes of the atmospheric circulation variability over the Euro-Atlantic region [32–35]. They are theoretically orthogonal and have different climate effects on the region [34,36]. These divergent views about the ENSO footprint in the early winter atmospheric circulation make it difficult to assess the ability of climate models to capture the true ENSO influence. ENSO-induced tropical convection anomalies, which are evident in almost all the tropical ocean basins, have been suggested to be the key factors for the early winter ENSO influence [14,15,17]. However, precipitation anomalies in different tropical ocean basins tend to have different extratropical effects [37,38]. In this case, this inconsistency may be related to an insufficient consideration of the respective roles of different tropical convection anomalies. The role of the monopolar anomalies in the western-central Indian Ocean (WCIO) [38,39], the western Pacific [16], and the central-eastern Pacific [18,38], as well as the dipolar convection anomalies over the tropical western–eastern Indian Ocean (TWEIO) [15,17] and over the Gulf of Mexico–Caribbean Sea (GMCA) [14,40], needs to be quantified and compared. In addition, the late winter ENSO–NAO teleconnection has been reported to show prominent interdecadal variations [5,41]. How the early winter ENSO teleconnection has changed in the recent decades is also an important scientific question to be addressed.

Considering the above scientific issues, we revisited the ENSO influence on the early winter Euro-Atlantic atmospheric circulation in this study. Based on the latest reanalysis datasets from 1979 to 2022, we show that the early winter ENSO signal projects better onto the EAP rather than onto the NAO, which is frequently mentioned previously. We further suggest that this ENSO–EAP relationship is evidently intensified during the past two decades. Possible mechanisms responsible for this ENSO influence and its interdecadal change are also proposed. In the remainder of the article, Section 2 describes the data and methodology, Section 3 provides the results and possible mechanisms, and the conclusions and discussion are summarized in Section 4.

2. Data and Methodology

In this study, the monthly datasets (1979–2022) used include global SST from the Hadley Centre sea ice and SST dataset (HadISST) version 1.1 with the horizontal resolution of 1° longitude × 1° latitude [42]. The precipitation and atmospheric circulation datasets are derived from the fifth generation of the European Centre for Medium-Range Weather Forecasts (ECMWF) Reanalysis (ERA5) [43] with the horizontal resolution of 1°

longitude × 1° latitude. To confirm our results, the atmospheric circulation was also examined based on the National Centers for Environmental Prediction/National Center for Atmospheric Research (NCEP/NCAR) Reanalysis dataset with a horizontal resolution of 2.5° × 2.5° [44] and the Japanese 55 year (JRA-55) Reanalysis dataset with a horizontal resolution of 1.25° × 1.25° [45]. We also utilized the monthly CMAP precipitation dataset (2.5° × 2.5°) [46], which is a combination of various satellite estimates and gauge data.

We focused the analysis mainly on the boreal winter season (November–March, ND-JFM), and unless explicitly stated, the winter of 2000 represents the average from November 2000 to March 2001. The early winter in this study denotes the two-month means of November–December. Anomalies were calculated relative to the monthly mean climatology over the entire period we used (1979–2022). To exclude the possible effects associated with global warming or long-term trends, the linear trends in all variables were removed. Statistical significance tests were performed using the two-tailed Student's *t*-test.

Several climatic indices were employed to facilitate our analyses. The Niño-3.4 index, which is defined as the area-averaged SST anomalies in the Niño-3.4 region (5° S–5° N, 120°–170° W), was used to measure the amplitude of ENSO. A threshold of ±0.5 standard deviations of the December to February (DJF) average Niño-3.4 index defines ENSO winters. This method identifies 14 El Niño winters, i.e., 1982, 1986, 1987, 1991, 1994, 1997, 2002, 2004, 2006, 2009, 2014, 2015, 2018, and 2019, and 15 La Niña winters, i.e., 1983, 1984, 1985, 1988, 1995, 1998, 1999, 2000, 2005, 2007, 2008, 2010, 2011, 2017, and 2020. The horizontal wave activity flux (WAF) developed by Takaya and Nakamura [47] was applied to analyze the source and direction of Rossby wave energy propagation. It is defined as

$$F = \frac{p \cos \varphi}{2|U|} \begin{cases} \frac{U}{a^2 \cos^2 \varphi} \left[\left(\frac{\partial \psi'}{\partial \lambda} \right)^2 - \psi' \frac{\partial^2 \psi'}{\partial \lambda^2} \right] + \frac{V}{a^2 \cos \phi} \left(\frac{\partial \psi'}{\partial \lambda} \frac{\partial \psi'}{\partial \varphi} - \psi' \frac{\partial^2 \psi'}{\partial \lambda \partial \varphi} \right) \\ \frac{U}{a^2 \cos \varphi} \left(\frac{\partial \psi'}{\partial \lambda} \frac{\partial \psi'}{\partial \varphi} - \psi' \frac{\partial^2 \psi'}{\partial \lambda \partial \varphi} \right) + \frac{V}{a^2} \left[\left(\frac{\partial \psi'}{\partial \varphi} \right)^2 - \psi' \frac{\partial^2 \psi'}{\partial \varphi^2} \right] \end{cases} \quad (1)$$

where F is the WAF; p is the pressure normalized to 1000 hPa; φ is the latitude; λ is the longitude; and a is the radius of the Earth. The geostrophic stream function ψ is defined as z/f, where z is the geopotential, and f (=$2\Omega sin\varphi$) is the Coriolis parameter with the Earth's rotation rate (Ω). Also, $|U|$, U, and V represent the basic states of wind speed, zonal, and meridional wind, respectively, while ψ' denotes the perturbed stream function. Since the Coriolis parameter approaches zero near the equator, the WAF is not calculated or plotted within the latitudes of 10° S–10° N.

3. Results

3.1. Early Winter ENSO Teleconnection over the Euro-Atlantic Sector

Considering that both the NAO [15,17] and EAP [30,31] have been proposed to be related to the ENSO forcing in early winter, we first performed an empirical orthogonal function (EOF) analysis of the SLP anomalies over the Euro-Atlantic region (25–80° N, 70° W–40° E) to describe these two modes in Figure 1. The first mode was consisted of a north–south dipole of the SLP anomalies near Iceland and the Azores, showing a distinct NAO-like pattern. The second mode also showed a north-south dipole of anomaly centers spanning the North Atlantic from east to west, but its anomaly centers were shifted southeast to the approximate nodal lines of the NAO pattern, referred to as the EAP mode. These results are consistent with previous studies [33,35,48] and remained unchanged when using different reanalysis datasets such as the NECP/NCAR (Figure S1) and the JRA-55 (Figure S2). The NAO and EAP indices are thus defined as the standardized first and second time series of these two modes, respectively. Note that we define the positive EAP pattern here as characterized by the center south of Iceland showing low pressure anomalies.
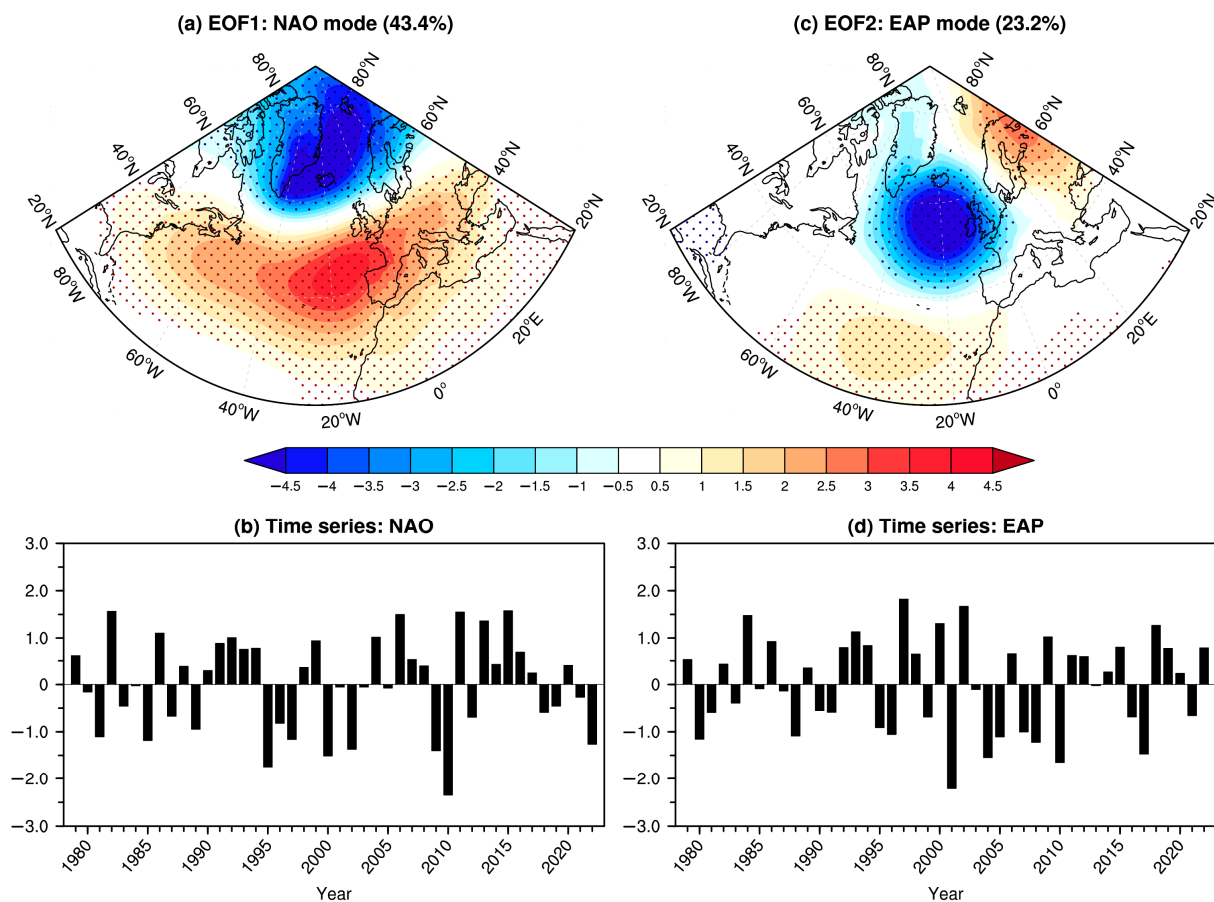
Figure 1. The (**a**) first and (**c**) second EOF spatial patterns (shading in hPa) and the corresponding (**b**) first and (**d**) second normalized time series (representing the NAO and EAP indices, respectively) of the early winter SLP anomalies in the North Atlantic region during 1979–2022. The percentages in (**a**,**b**) are the variability explained by the corresponding EOF. The dots in (**b**) indicate the anomalies exceeding the 95% confidence level.

To reassess the influence of ENSO, Figure 2a illustrates the spatial pattern of the early winter SLP anomalies regressed onto the Niño-3.4 index. It shows a dipolar SLP pattern over the North Atlantic, with the negative anomaly located to the south of Iceland and west of Ireland, and the positive anomaly located in the subtropics. When comparing this pattern (Figure 2a) with the NAO and EAP (Figure 1a,c), it becomes evident that it aligns more closely with the EAP than with the NAO. The pattern correlation coefficients of the ENSO-regressed SLP spatial distribution with the NAO and EAP patterns over the Euro-Atlantic region were 0.57 and 0.77, respectively. And the temporal correlation coefficients of the Niño-3.4 index with the NAO and EAP indices were, respectively, 0.18 and 0.45 (Figure 2b). While the ENSO-NAO relationship was weak, the latter was strong and significant at the 95% confidence level, suggesting that ENSO could exert a robust in-phase influence on the early winter EAP. The close relationship between the ENSO and EAP was also manifested in the high pattern similarity of their associated tropical precipitation anomalies (Figure 2c,d). A warm ENSO event can induce a strong positive precipitation anomaly in the central-eastern tropical Pacific, the western-central Indian Ocean, and the Gulf of Mexico. Meanwhile, negative precipitation anomaly was detected in the western Pacific and the Caribbean Sea. These precipitation anomalies were also accompanied by a positive EAP pattern. As suggested by previous studies [14,15,17], during early winter, ENSO-induced tropical convection anomalies play a key role in transmitting the ENSO signal to the North Atlantic. We can therefore infer that the precipitation anomalies marked in Figure 2c,d may be important for the ENSO–EAP teleconnection.
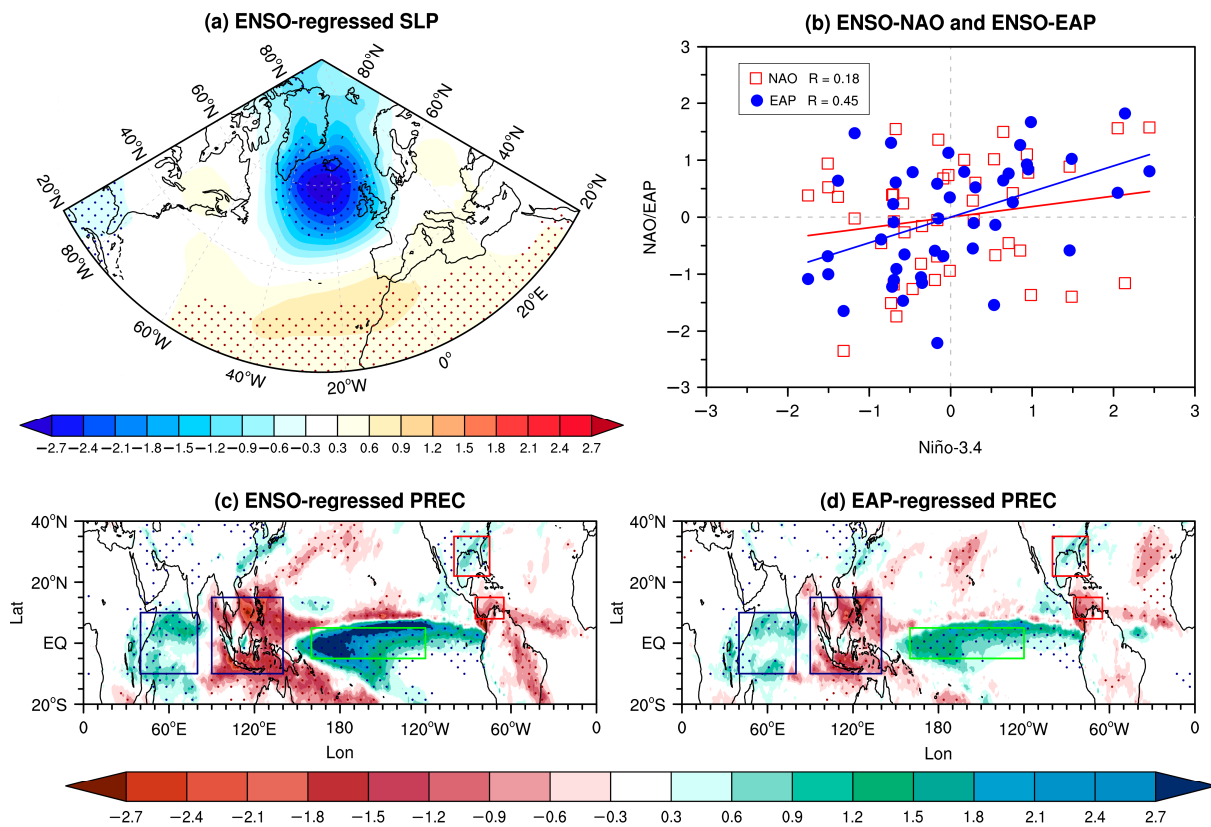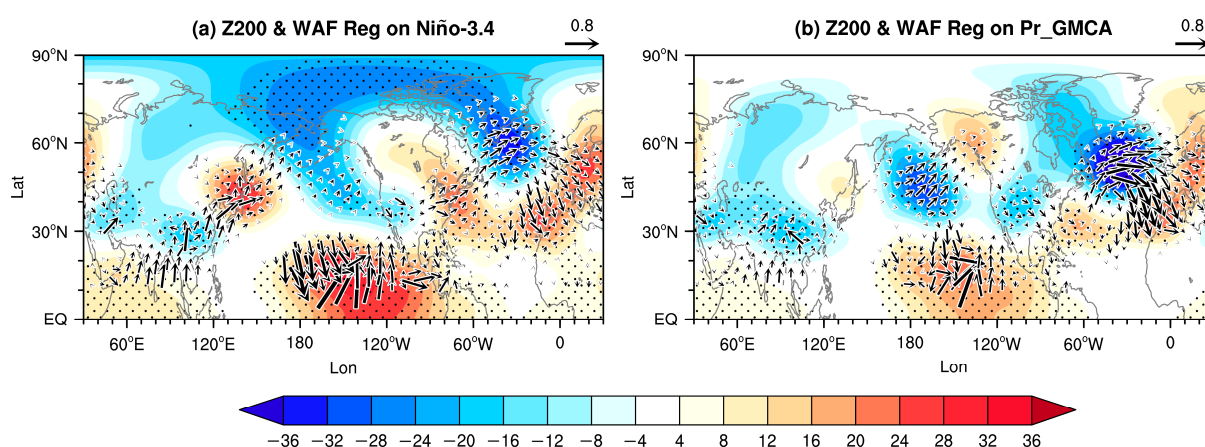
Figure 2. (**a**) Regression coefficients of the early winter North Atlantic SLP anomalies (shading in hPa) with respect to the DJF Niño-3.4 index. (**b**) Scatterplot of the early winter NAO (red quadrate) and EAP (blue circle) indices with the DJF Niño-3.4 index with the corresponding linear regression lines. The correlation coefficients (R) of the NAO and EAP indices with the Niño-3.4 index are also displayed. (**c**) Regression coefficients of the early winter tropical precipitation anomalies (shading in mmday^{-1}) with respect to the DJF Niño-3.4 index. (**d**) is the same as (**c**) but for the regression coefficients with respect to the early winter EAP index. The dots in (**a,c,d**) indicate the anomalies exceeding the 95% confidence level. The navy, green, and red boxes in (**c,d**) mark the domains used to define the Pr_TWEIO, Pr_CP, and Pr_GMCA indices, respectively.

To understand the relative role of these ENSO-related tropical precipitation anomalies in the early winter ENSO teleconnection, we define three precipitation indices according to Figure 2c,d. The tropical western-eastern Indian Ocean dipolar precipitation index (Pr_TWEIO) is defined as the difference between the area-averaged precipitation anomaly over the tropical western (10° S–10° N, 40°–80° E) and eastern (10° S–15° N, 90°–140° E) Indian Oceans. The tropical central Pacific index (Pr_CP) is represented by the area-averaged precipitation anomaly in the tropical central Pacific (5° S–5° N, 160° E–180°–120° W). And the dipolar GMCA precipitation index (Pr_GMCA) is defined as the difference between the area-averaged precipitation anomaly over the Gulf of Mexico (22°–35° N, 75°–100° W) and the Caribbean Sea (5°–18° N, 65°–85° W). The definitions of these three indices basically follow those used in previous studies [14,15,18]. All of these three indices showed a significant relationship with the EAP (Table 1). In order to examine their individual effect, we performed a multiple regression analysis. It was found that the independent effects of the Pr_CP and Pr_TWEIO indices were no longer significant at the 95% confidence level. Only the Pr_GMCA index, with a regression coefficient of 0.50, was still able to have an independent significant influence on the EAP. This Pr_GMCA index alone can explain 35% of the total variance of the EAP, suggesting that the precipitation anomalies in the GMCA may be the key bridge that transmits ENSO effects to the North Atlantic. To uncover the physical processes by which the Pr_GMCA influences the EAP, in Figure 3, we

show the regressed early winter 200-hPa geopotential height anomalies and the associated WAF with respect to the Niño-3.4 and Pr_GMCA indices, respectively. For both cases, an evident positive geopotential height anomaly existed to the east of the Gulf of Mexico. Over there, a Rossby wave train formed and propagated northward, creating a negative anomaly to the south of Iceland and west of Ireland, resulting in a positive EAP. This strong similarity between the ENSO-regressed and Pr_GMCA-regressed patterns across the North Atlantic indicated that the PR_GMCA played an important role in creating the ENSO–EAP teleconnection in early winter by exciting a Rossby wave train. These results remained essentially unchanged when the CMAP precipitation dataset was utilized (Figure S3), and were generally in good agreement with previous studies that also underscore the role of the Pr_GMCA [14,41], although they do not mention the ENSO–EAP relationship.

Table 1. Regressed and partially regressed EAP index onto the tropical precipitation indices. The value marked with an asterisk indicates that it is significant at the 95% confidence level.

	Pr_CP	Pr_TWEIO	Pr_GMCA
Regressed EAP index	0.46 *	0.51 *	0.59 *
Partially regressed EAP index	−0.12	0.35	0.50 *

Figure 3. Regression coefficients of the early winter 200 hPa geopotential height anomalies (shading in m) and the associated anomalous wave activity flux (WAF, vectors in m^2s^{-2}) with respect to the (**a**) DJF Niño-3.4 and (**b**) early winter Pr_GMCA indices. The dots denote the geopotential height anomalies exceeding the 95% confidence level. The anomalous WAF flux is shown only when its magnitude is larger than 0.1 m^2s^{-2}.

3.2. Interdecadal Strengthening of the ENSO–EAP Relationship

To inspect the possible interdecadal change of the early winter ENSO–EAP teleconnection, Figure 4a shows the time evolution of the 21 year running correlation between the Niño-3.4 and EAP indices. We can see that the ENSO–EAP relationship underwent a pronounced interdecadal strengthening during the late 1990s. ENSO and EAP were significantly correlated after the late 1990s at the 95% confidence level (R = 0.51, Table 2), while a non-significant relationship was found before the late 1990s (R = 0.28, Table 2). The conclusions remained unchanged when we used other reanalysis datasets to calculate the EAP index (Figure 4a), or when we used different running time windows, such as 19 and 23 years (Figure S4).

(a) ENSO-EAP running correlation

(b) P1 (1979−1996) ENSO-regressed SLP

(c) P2 (1997−2022) ENSO-regressed SLP
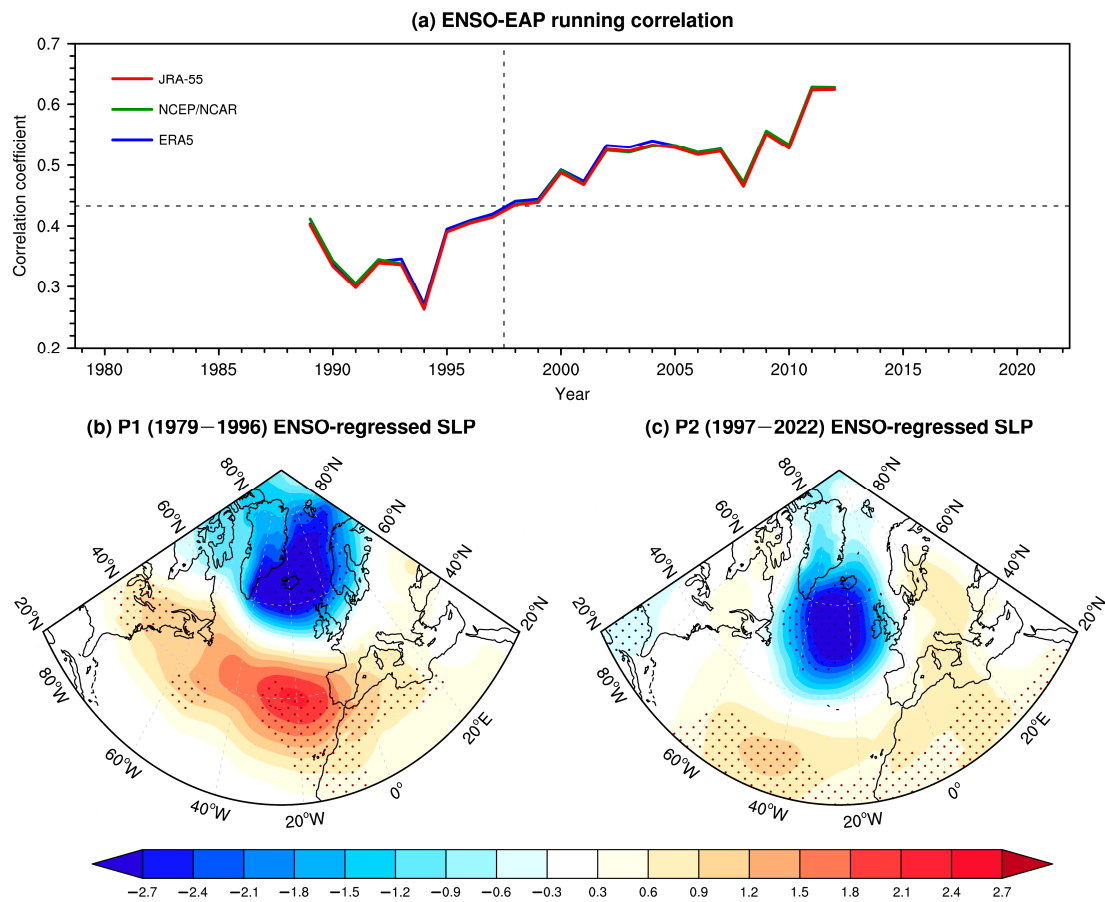
Figure 4. (**a**) The 21 year running correlation coefficients between the DJF Niño-3.4 index and early winter EAP index during 1979–2022 based on the JRA-55 (red curve), NCEP/NCAR (green curve), and ERA5 (blue curve) reanalysis datasets. The horizontal gray dashed line indicates the 95% confidence level for the correlation. Regression coefficients of the early winter North Atlantic SLP anomalies (shading in hPa) with respect to the DJF Niño-3.4 index during (**b**) 1979–1996 (denoted as P1) and (**c**) 1997–2022 (denoted as P2). The dots in (**b**,**c**) indicate the anomalies exceeding the 95% confidence level.

Table 2. Correlation coefficients between the Niño-3.4 index and the early winter Euro-Atlantic atmospheric modes. The value marked with an asterisk indicates that it is significant at the 95% confidence level.

	P1 (1979–1996)	P2 (1997–2022)
Cor. (Niño-3.4, EAP)	0.28	0.51 *
Cor. (Niño-3.4, NAO)	0.57 *	0.10

According to Figure 4a, we then refer to the period from 1979 to 1996 as P1 and the period from 1999 to 2022 as P2 for further investigation. The spatial patterns of the ENSO-regressed early winter SLP anomalies during these two periods are shown in Figure 4b,c, respectively. It is interesting to note that while the pattern in P2 resembles the positive EAP pattern, the pattern in P1 projects well onto the NAO. The pattern correlation coefficients between the P1 pattern and the NAO pattern and between the P2 pattern and the EAP pattern over the Euro-Atlantic region were 0.92 and 0.86, respectively. These results suggest that the early winter ENSO teleconnection to the Euro-Atlantic changed its pattern from NAO to EAP around the late 1990s (Table 2).

3.3. Possible Mechanism

We now turn to an analysis of the possible reasons that are responsible for this interdecadal change. In Figure 5, the spatial patterns of the ENSO-regressed tropical SST, 850 hPa wind, and precipitation anomalies during P1 and P2 are examined. While the typical ENSO-related SST, low-level wind, and precipitation anomalies were present in the Pacific on a broad scale, differences can be found in the details. Compared to the SST in P1, there were significant warm SST anomalies in the subtropical and tropical northeastern Pacific in P2. Correspondingly, the precipitation responses in the tropical eastern Pacific were apparently stronger than that in P1. As a direct response to the atmospheric anomaly generated by the warm SST anomaly in the eastern Pacific, the precipitation was reduced in the Caribbean Sea [49,50], also with a stronger magnitude in P2. In response to this reduced convection, a stronger anticyclonic circulation developed over the subtropical western North Atlantic (Figure 5b), leading to a stronger precipitation surplus in the Gulf of Mexico in P2. We then compared the ENSO-induced tropical precipitation anomalies during P1 and P2 in Table 3. Although the precipitation response in the CP and TWEIO remained almost unchanged from P1 to P2, a significant enhancement of the precipitation response in P2 was found in the GMCA, which was the key region for creating an effective ENSO–EAP teleconnection as we demonstrated in the previous section. Therefore, we suggest that the intensification of the Pr_GMCA response to ENSO in P2 was responsible for the interdecadal strengthening of the ENSO–EAP relationship.
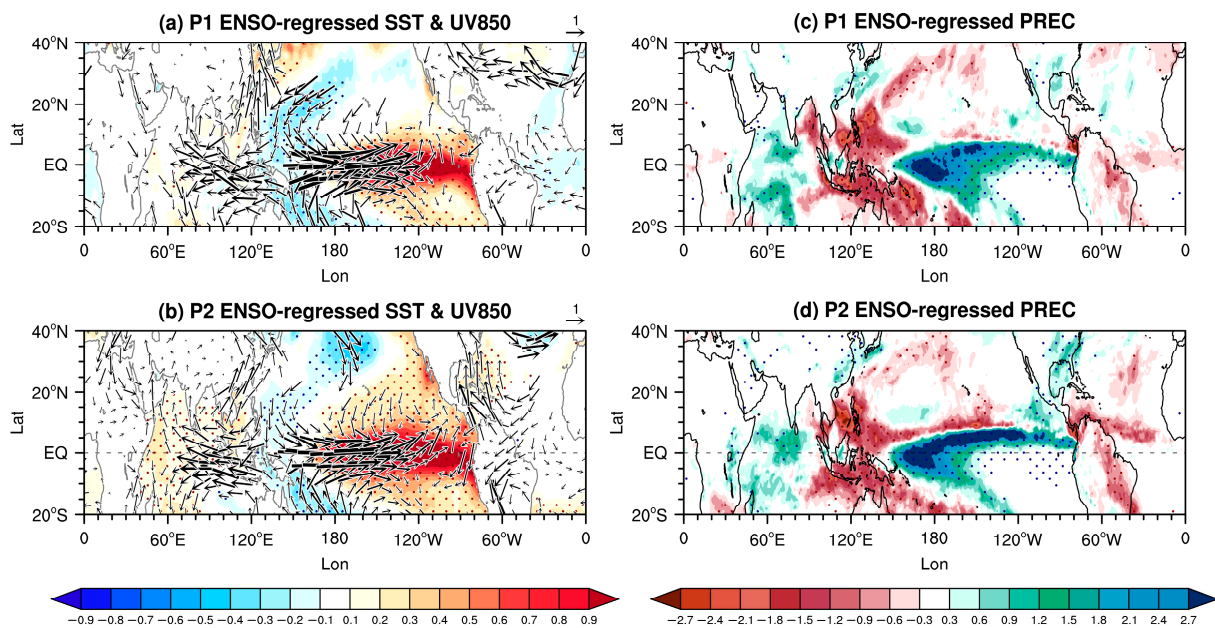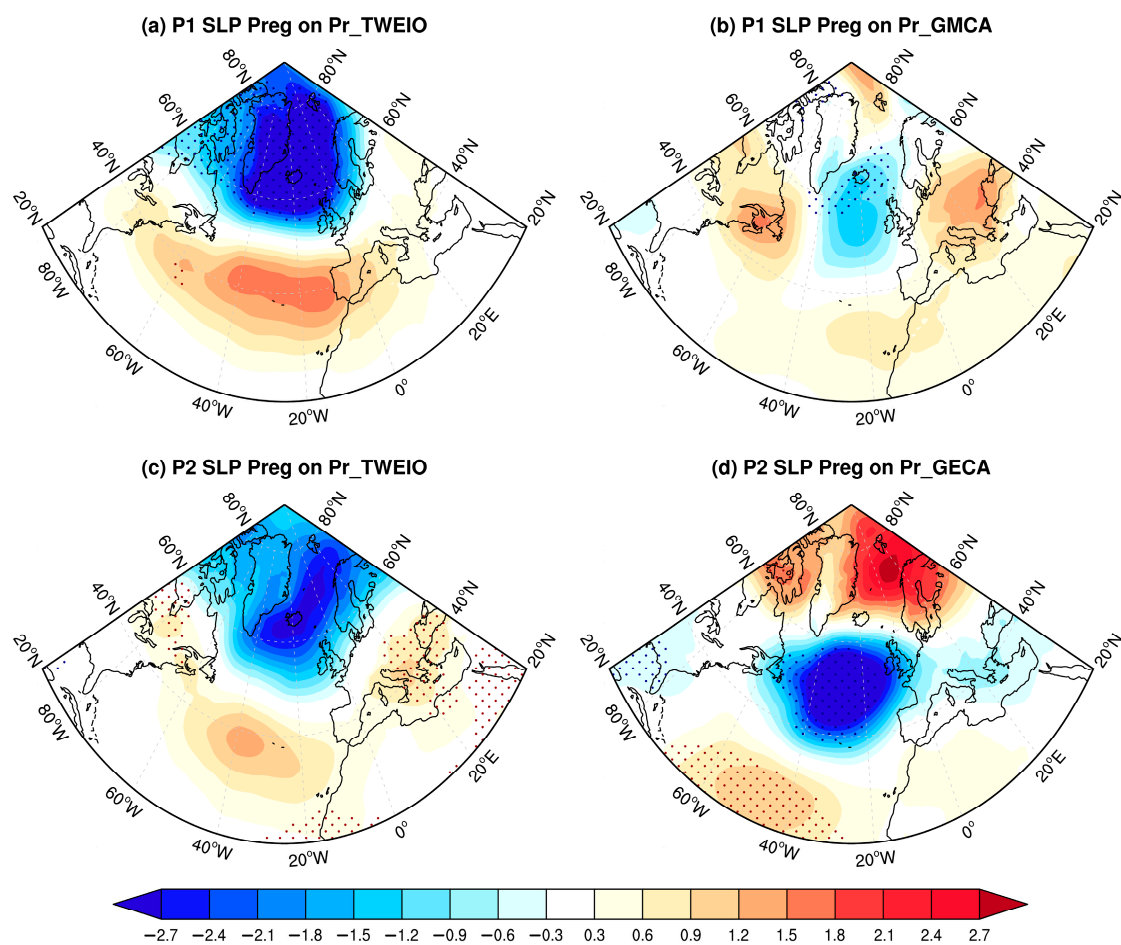

Figure 5. Regression coefficients of the early winter (**a**,**b**) SST (shading in K), 850 hPa wind (vectors in m/s), and (**c**,**d**) precipitation (shading in mmday^{-1}) anomalies with respect to the DJF Niño-3.4 index during (**a**,**c**) P1 and (**b**,**d**) P2. The dots indicate the anomalies exceeding the 95% confidence level. The 850 hPa wind anomaly is shown only when its zonal or meridional component is significant at the 95% confidence level.

Table 3. ENSO-regressed tropical precipitation indices (units: mmday^{-1}) during P1 and P2. The value marked with an asterisk indicates that it was significant at the 95% confidence level.

|	Pr_CP	Pr_TWEIO	Pr_GMCA
P1 (1979–1996)	1.90 *	1.52 *	0.69 *
P2 (1997–2022)	1.84 *	1.52 *	1.29 *

Previous studies have demonstrated that the tropical Indian Ocean dipolar precipitation is also important for establishing the early winter ENSO teleconnection to the Euro-Atlantic [15,17]. To examine the role of Pr_GMCA and Pr_TWEIO, we show the partial regression patterns of the Euro-Atlantic early winter SLP anomalies with respect to the Pr_TWEIO and Pr_GMCA indices during P1 and P2 in Figure 6. During P1, due to the weak response of the Pr_GMCA to ENSO, its effect on the Euro-Atlantic SLP was relatively weak. The ENSO influence was mainly contributed by the tropical precipitation forcing in the Indian Ocean, which favored a positive NAO pattern. This is in agreement with previous studies [15,17]. However, during P2, we can clearly see that the effect of the Pr_GMCA significantly strengthened, which was well projected onto the EAP. Although the Pr_TWEIO was still at work and favored an NAO response, the ENSO influence was dominated by the Pr_GMCA, and finally a positive EAP was generated. These results suggest that the magnitude of the ENSO-induced precipitation anomaly in the GMCA is crucial for the ENSO–EAP teleconnection.

Figure 6. Partial regression coefficients of the Euro-Atlantic SLP anomalies (shading in hPa) with respect to the (**a**) Pr_TWEIO and (**b**) Pr_GMCA indices during P1. (**c**,**d**) are the same as (**a**,**b**) but during P2. The dots indicate the SLP anomalies exceeding the 95% confidence level.

To further understand the role of the precipitation anomaly in the GMCA, Figure 7 displays the relationships between the Niño-3.4 and Pr_GMCA indices, and between the Pr_GMCA and EAP indices during the ENSO early winter months for P1 and P2. We can clearly see that the ENSO events in P2 were able to generate stronger precipitation anomalies in the GMCA in P2 compared to those in P1 (Figure 7a). This stronger Pr_GMCA response, in turn, was able to effectively establish a Rossby wave train that led to an EAP anomaly. The stronger the ENSO-induced precipitation anomaly in the GMCA, the more

robust the EAP response, and also the ENSO–EAP teleconnection can be produced during the ENSO early winter (Figure 7b). However, in P1, the precipitation response was too weak to excite a clear Rossby wave bridging ENSO and the Euro-Atlantic atmospheric pattern. The EAP variability may be influenced by other climate drivers, so we were unable to observe a significant relationship between the Pr_GMCA and the EAP. These findings were qualitatively consistent when using the CMAP precipitation dataset (Figures S5 and S6). In summary, we conclude that the Pr_GMCA played a key role in shaping the ENSO–EAP teleconnection during early winter.
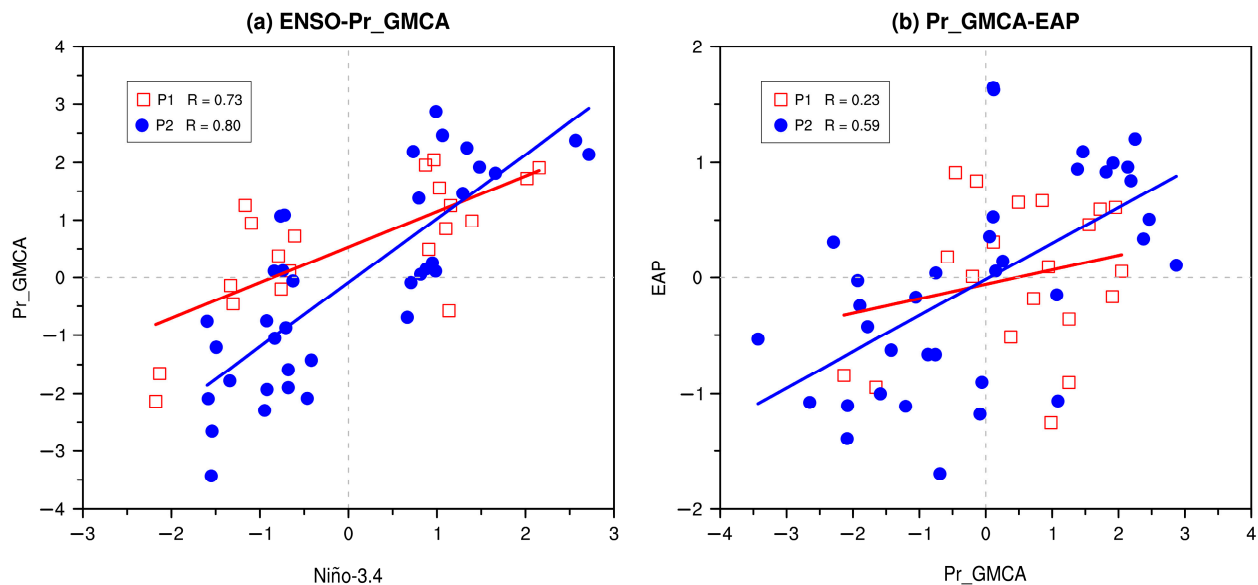
Figure 7. (**a**) Scatterplot of the early winter monthly Pr_GMCA and Niño-3.4 indices for the ENSO winters during P1 (red quadrate) and P2 (blue circle) with the corresponding linear regression lines. (**b**) Scatterplot the early winter monthly EAP and Pr_GMCA indices for the ENSO winters during P1 (red quadrate) and P2 (blue circle). The correlation coefficients (R) are also displayed.

4. Conclusions and Discussion

Previous studies have shown that the ENSO teleconnection to the Euro-Atlantic sector is subject to considerable subseasonal transitions [13–15]. Compared with the late winter ENSO impacts that display a negative (positive) NAO during El Niño (La Niña), the early winter ENSO teleconnection is less understood. In this study, based on the multiple reanalysis datasets, we revisited the ENSO influence on the early winter Euro-Atlantic atmospheric circulation during the 1979–2022 period. It was found that the ENSO footprint fitted the EAP much better than the frequently mentioned NAO pattern. This influence was associated with ENSO-induced dipolar convection anomalies over the GMCA region, which can set up a Rossby wave train propagating northward into the North Atlantic, leading to a low-pressure anomaly south of Iceland and west of Ireland in El Niño cases, and thus a positive EAP.

We then examined the possible interdecadal change of this early winter ENSO tele-connection. It was revealed that the ENSO–EAP relationship underwent a pronounced interdecadal strengthening around the late 1990s. While a clear EAP response was detected during ENSO early winter after the late 1990s, the ENSO-regressed pattern resembled a NAO pattern before the late 1990s, suggesting that there was a shift of the early winter ENSO teleconnection over the Euro-Atlantic sector around the late 1990s. We assume that the changing response of the GMCA precipitation to ENSO played a key role in this inter-decadal shift. Prior to the late 1990s, the ENSO-related GMCA precipitation anomaly was weak, unable to exert an effective influence on the Euro-Atlantic atmospheric circulation. The ENSO teleconnection to this region was mainly contributed to by the precipitation

anomaly in the TWEIO, which favored a NAO anomaly. In contrast, the GMCA precipitation response to ENSO has been strongly enhanced since the late 1990s. Although the TWEIO precipitation forcing is still at work, the role of the GMCA precipitation overwhelms and eventually produces an EAP by exciting a north-propagating Rossby wave train.

Our results are consistent with those of Thornton et al. [48], who demonstrated a visible but weak seasonal predictability of the ENSO-related EAP and surface climate over the Euro-Atlantic in early winter. This weaker signal is suggested to be caused by the weaker model simulation of tropical–extratropical teleconnections [48], which in turn seems to be related to the underestimated convection response to ENSO in the GMCA region [14,40]. Our results highlight the role of the GMCA precipitation in the ENSO–EAP teleconnection and thus confirm these arguments. In addition, the conclusion of the recent ENSO–EAP teleconnection strengthening indicates a pattern shift of the ENSO fingerprint on the Euro-Atlantic early winter atmospheric circulation. These results are important for understanding the ENSO teleconnection in early winter and also important for improving the seasonal climate prediction over the Euro-Atlantic region.

We note that our results are mostly based on the observational analysis, and that evidence from modeling and CMIP6 simulations need to be presented in the future. In this study, we mainly focused on the role of ENSO-induced low-frequency Rossby waves. However, the North Atlantic is a region of abundant atmospheric eddy-low frequency flow feedbacks [51]. Therefore, their possible effects may also need to be investigated [52,53]. In addition, this study mainly concentrated on the linear ENSO effects, and whether this teleconnection is sensitive to the type or diversity of ENSO needs to be clarified. Since the ENSO teleconnections are subject to significant changes under the future warming climate [54,55], the way in which they respond to greenhouse warming is also an interesting topic worthy of future study.

Conflicts of Interest: The authors declare no conflict of interest.

References

1. Ropelewski, C.F.; Halpert, M.S. Global and Regional Scale Precipitation Patterns Associated with the El Niño/Southern Oscillation. *Mon. Wea. Rev.* **1987**, *115*, 1606–1626. [CrossRef]
2. Trenberth, K.E.; Caron, J.M. The Southern Oscillation Revisited: Sea Level Pressures, Surface Temperatures, and Precipitation. *J. Clim.* **2000**, *13*, 4358–4365. [CrossRef]
3. Alexander, M.A.; Bladé, I.; Newman, M.; Lanzante, J.R.; Lau, N.-C.; Scott, J.D. The Atmospheric Bridge: The Influence of ENSO Teleconnections on Air–Sea Interaction over the Global Oceans. *J. Clim.* **2002**, *15*, 2205–2231. [CrossRef]
4. Brönnimann, S. Impact of El Niño–Southern Oscillation on European Climate. *Rev. Geophys.* **2007**, *45*, RG3003. [CrossRef]
5. López-Parages, J.; Rodríguez-Fonseca, B.; Terray, L. A Mechanism for the Multidecadal Modulation of ENSO Teleconnection with Europe. *Clim. Dyn.* **2015**, *45*, 867–880. [CrossRef]
6. Deser, C.; Simpson, I.R.; McKinnon, K.A.; Phillips, A.S. The Northern Hemisphere Extratropical Atmospheric Circulation Response to ENSO: How Well Do We Know It and How Do We Evaluate Models Accordingly? *J. Clim.* **2017**, *30*, 5059–5082. [CrossRef]
7. Zhang, W.; Wang, Z.; Stuecker, M.F.; Turner, A.G.; Jin, F.-F.; Geng, X. Impact of ENSO Longitudinal Position on Teleconnections to the NAO. *Clim. Dyn.* **2019**, *52*, 257–274. [CrossRef]
8. Toniazzo, T.; Scaife, A.A. The Influence of ENSO on Winter North Atlantic Climate. *Geophys. Res. Lett.* **2006**, *33*, L24704. [CrossRef]
9. Hardiman, S.C.; Dunstone, N.J.; Scaife, A.A.; Smith, D.M.; Ineson, S.; Lim, J.; Fereday, D. The Impact of Strong El Niño and La Niña Events on the North Atlantic. *Geophys. Res. Lett.* **2019**, *46*, 2874–2883. [CrossRef]
10. Jiménez-Esteve, B.; Domeisen, D.I.V. Nonlinearity in the North Pacific Atmospheric Response to a Linear ENSO Forcing. *Geophys. Res. Lett.* **2019**, *46*, 2271–2281. [CrossRef]
11. Graf, H.-F.; Zanchettin, D. Central Pacific El Niño, the "Subtropical Bridge," and Eurasian Climate. *J. Geophys. Res.* **2012**, *117*, D01102. [CrossRef]
12. Zhang, W.; Wang, L.; Xiang, B.; Qi, L.; He, J. Impacts of Two Types of La Niña on the NAO during Boreal Winter. *Clim. Dyn.* **2015**, *44*, 1351–1366. [CrossRef]
13. Moron, V.; Gouirand, I. Seasonal Modulation of the El Niño–Southern Oscillation Relationship with Sea Level Pressure Anomalies over the North Atlantic in October–March 1873–1996. *Int. J. Climatol.* **2003**, *23*, 143–155. [CrossRef]
14. Ayarzagüena, B.; Ineson, S.; Dunstone, N.J.; Baldwin, M.P.; Scaife, A.A. Intraseasonal Effects of El Niño–Southern Oscillation on North Atlantic Climate. *J. Clim.* **2018**, *31*, 8861–8873. [CrossRef]
15. Abid, M.A.; Kucharski, F.; Molteni, F.; Kang, I.-S.; Tompkins, A.M.; Almazroui, M. Separating the Indian and Pacific Ocean Impacts on the Euro-Atlantic Response to ENSO and Its Transition from Early to Late Winter. *J. Clim.* **2021**, *34*, 1531–1548. [CrossRef]
16. Bladé, I.; Newman, M.; Alexander, M.A.; Scott, J.D. The Late Fall Extratropical Response to ENSO: Sensitivity to Coupling and Convection in the Tropical West Pacific. *J. Clim.* **2008**, *21*, 6101–6118. [CrossRef]
17. Joshi, M.K.; Abid, M.A.; Kucharski, F. The Role of an Indian Ocean Heating Dipole in the ENSO Teleconnection to the North Atlantic European Region in Early Winter during the Twentieth Century in Reanalysis and CMIP5 Simulations. *J. Clim.* **2021**, *34*, 1047–1060. [CrossRef]
18. Geng, X.; Zhao, J.; Kug, J.-S. ENSO-Driven Abrupt Phase Shift in North Atlantic Oscillation in Early January. *NPJ Clim. Atmos. Sci.* **2023**, *6*, 80. [CrossRef]
19. Ineson, S.; Scaife, A.A. The Role of the Stratosphere in the European Climate Response to El Niño. *Nat. Geosci.* **2009**, *2*, 32–36. [CrossRef]
20. Jiménez-Esteve, B.; Domeisen, D.I.V. The Tropospheric Pathway of the ENSO–North Atlantic Teleconnection. *J. Clim.* **2018**, *31*, 4563–4584. [CrossRef]
21. Sung, M.-K.; Ham, Y.-G.; Kug, J.-S.; An, S.-I. An Alterative Effect by the Tropical North Atlantic SST in Intraseasonally Varying El Niño Teleconnection over the North Atlantic. *Tellus A Dyn. Meteorol. Oceanogr.* **2013**, *65*, 19863. [CrossRef]
22. Ham, Y.-G.; Sung, M.-K.; An, S.-I.; Schubert, S.D.; Kug, J.-S. Role of Tropical Atlantic SST Variability as a Modulator of El Niño Teleconnections. *Asia-Pac. J. Atmos. Sci.* **2014**, *50*, 247–261. [CrossRef]
23. Li, Y.; Lau, N.-C. Impact of ENSO on the Atmospheric Variability over the North Atlantic in Late Winter—Role of Transient Eddies. *J. Clim.* **2012**, *25*, 320–342. [CrossRef]
24. Cagnazzo, C.; Manzini, E. Impact of the Stratosphere on the Winter Tropospheric Teleconnections between ENSO and the North Atlantic and European Region. *J. Clim.* **2009**, *22*, 1223–1238. [CrossRef]
25. Bell, C.J.; Gray, L.J.; Charlton-Perez, A.J.; Joshi, M.M.; Scaife, A.A. Stratospheric Communication of El Niño Teleconnections to European Winter. *J. Clim.* **2009**, *22*, 4083–4096. [CrossRef]
26. Tippett, M.K.; Barnston, A.G.; Li, S. Performance of recent multimodel ENSO forecasts. *J. App Meteorol. Clim.* **2012**, *51*, 637–654. [CrossRef]

27.   Muhammad, A.E.; L'Heureux, M.; Tippett, M.; Robertson, A.; Turmelle, J. Real-Time ENSO Forecast Skill Evaluated Over the Last Two Decades, with Focus on Onset of ENSO Events, 15 November 2023, PREPRINT (Version 1). Available online: https://doi.org/10.21203/rs.3.rs-3588191/v1 (accessed on 23 November 2023).

28.   Molteni, F.; Roberts, C.D.; Senan, R.; Keeley, S.P.E.; Bellucci, A.; Corti, S.; Fuentes Franco, R.; Haarsma, R.; Levine, X.; Putrasahan, D.; et al. Boreal-Winter Teleconnections with Tropical Indo-Pacific Rainfall in HighResMIP Historical Simulations from the PRIMAVERA Project. *Clim. Dyn.* **2020**, *55*, 1843–1873. [CrossRef]

29.   Molteni, F.; Brookshaw, A. Early- and Late-Winter ENSO Teleconnections to the Euro-Atlantic Region in State-of-the-Art Seasonal Forecasting Systems. *Clim. Dyn.* **2023**, *61*, 2673–2692. [CrossRef]

30.   King, M.P.; Herceg-Bulić, I.; Kucharski, F.; Keenlyside, N. Interannual Tropical Pacific Sea Surface Temperature Anomalies Teleconnection to Northern Hemisphere Atmosphere in November. *Clim. Dyn.* **2018**, *50*, 1881–1899. [CrossRef]

31.   King, M.P.; Herceg-Bulić, I.; Bladé, I.; García-Serrano, J.; Keenlyside, N.; Kucharski, F.; Li, C.; Sobolowski, S. Importance of Late Fall ENSO Teleconnection in the Euro-Atlantic Sector. *Bull. Am. Meteorol. Soc.* **2018**, *99*, 1337–1343. [CrossRef]

32.   Wallace, J.M.; Gutzler, D.S. Teleconnections in the Geopotential Height Field during the Northern Hemisphere Winter. *Mon. Weather Rev.* **1981**, *109*, 784–812. [CrossRef]

33.   Barnston, A.G.; Livezey, R.E. Classification, Seasonality and Persistence of Low-Frequency Atmospheric Circulation Patterns. *Mon. Wea. Rev.* **1987**, *115*, 1083–1126. [CrossRef]

34.   Hurrell, J.W. Decadal Trends in the North Atlantic Oscillation: Regional Temperatures and Precipitation. *Science* **1995**, *269*, 676–679. [CrossRef] [PubMed]

35.   Comas-Bru, L.; Hernández, A. Reconciling North Atlantic Climate Modes: Revised Monthly Indices for the East Atlantic and the Scandinavian Patterns beyond the 20th Century. *Earth Syst. Sci. Data* **2018**, *10*, 2329–2344. [CrossRef]

36.   Rodriguez-Puebla, C.; Encinas, A.H.; Nieto, S.; Garmendia, J. Spatial and Temporal Patterns of Annual Precipitation Variability over the Iberian Peninsula. *Int. J. Climatol.* **1998**, *18*, 299–316. [CrossRef]

37.   Scaife, A.A.; Comer, R.E.; Dunstone, N.J.; Knight, J.R.; Smith, D.M.; MacLachlan, C.; Martin, N.; Peterson, K.A.; Rowlands, D.; Carroll, E.B.; et al. Tropical rainfall, Rossby waves and regional winter climate predictions. *Q. J. R. Meteorol. Soc.* **2017**, *143*, 1–11. [CrossRef]

38.   Fletcher, C.G.; Cassou, C. The dynamical influence of separate teleconnections from the Pacific and Indian Oceans on the northern annular mode. *J. Clim.* **2015**, *28*, 7985–8002. [CrossRef]

39.   Abid, M.A.; Kucharski, F.; Molteni, F.; Almazroui, M. Predictability of Indian Ocean Precipitation and Its North Atlantic Teleconnections during Early Winter. *NPJ Clim. Atmos. Sci.* **2023**, *6*, 17. [CrossRef]

40.   Li, R.K.K.; Woollings, T.; O'Reilly, C.; Scaife, A.A. Effect of the North Pacific Tropospheric Waveguide on the Fidelity of Model El Niño Teleconnections. *J. Clim.* **2020**, *33*, 5223–5237. [CrossRef]

41.   Ivasić, S.; Herceg-Bulić, I.; King, M.P. Recent Weakening in the Winter ENSO Teleconnection over the North Atlantic-European Region. *Clim. Dyn.* **2021**, *57*, 1953–1972. [CrossRef]

42.   Rayner, N.A.; Parker, D.E.; Horton, E.B.; Folland, C.K.; Alexander, L.V.; Rowell, D.P.; Kent, E.C.; Kaplan, A. Global Analyses of Sea Surface Temperature, Sea Ice, and Night Marine Air Temperature since the Late Nineteenth Century. *J. Geophys. Res. Atmos.* **2003**, *108*, 4407. [CrossRef]

43.   Hersbach, H.; Bell, B.; Berrisford, P.; Hirahara, S.; Horányi, A.; Muñoz-Sabater, J.; Nicolas, J.; Peubey, C.; Radu, R.; Schepers, D.; et al. The ERA5 Global Reanalysis. *Q. J. R. Meteorol. Soc.* **2020**, *146*, 1999–2049. [CrossRef]

44.   Kalnay, E.; Kanamitsu, M.; Kistler, R.; Collins, W.; Deaven, D.; Gandin, L.; Iredell, M.; Saha, S.; White, G.; Woollen, J.; et al. The NCEP/NCAR 40-Year Reanalysis Project. *Bull. Am. Meteorol. Soc.* **1996**, *77*, 437–471. [CrossRef]

45.   Kobayashi, S.; Ota, Y.; Harada, Y.; Ebita, A.; Moriya, M.; Onoda, H.; Onogi, K.; Kamahori, H.; Kobayashi, C.; Endo, H.; et al. The JRA-55 Reanalysis: General Specifications and Basic Characteristics. *J. Meteorol. Soc. Japan. Ser. II* **2015**, *93*, 5–48. [CrossRef]

46.   Xie, P.; Arkin, P.A. Global precipitation: A 17-year monthly analysis based on gauge observations, satellite estimates, and numerical model outputs. *Bull. Am. Meteorol. Soc.* **1997**, *78*, 2539–2558. [CrossRef]

47.   Takaya, K.; Nakamura, H. A Formulation of a Phase-Independent Wave-Activity Flux for Stationary and Migratory Quasi-geostrophic Eddies on a Zonally Varying Basic Flow. *J. Atmos. Sci.* **2001**, *58*, 608–627. [CrossRef]

48.   Thornton, H.E.; Smith, D.M.; Scaife, A.A.; Dunstone, N.J. Seasonal Predictability of the East Atlantic Pattern in Late Autumn and Early Winter. *Geophys. Res. Lett.* **2023**, *50*, e2022GL100712. [CrossRef]

49.   Giannini, A.; Kushnir, Y.; Cane, M.A. Interannual Variability of Caribbean Rainfall, ENSO, and the Atlantic Ocean. *J. Clim.* **2000**, *13*, 297–311. [CrossRef]

50.   Giannini, A.; Kushnir, Y.; Cane, M.A. Seasonality in the Impact of ENSO and the North Atlantic High on Caribbean Rainfall. *Phys. Chem. Earth Part B Hydrol. Ocean. Atmos.* **2001**, *26*, 143–147. [CrossRef]

51.   Kug, J.S.; Jin, F.F. Left-hand rule for synoptic eddy feedback on low-frequency flow. *Geophys. Res. Lett.* **2009**, *36*, L05709. [CrossRef]

52.   Scaife, A.A.; Camp, J.; Comer, R.; Davis, P.; Dunstone, N.; Gordon, M.; MacLachlan, C.; Martin, N.; Nie, Y.; Ren, H.-L.; et al. Does Increased Atmospheric Resolution Improve Seasonal Climate Predictions? *Atmos. Sci. Lett.* **2019**, *20*, e922. [CrossRef]

53.   Hardiman, S.C.; Dunstone, N.J.; Scaife, A.A.; Smith, D.M.; Comer, R.; Nie, Y.; Ren, H.-L. Missing Eddy Feedback May Explain Weak Signal-to-Noise Ratios in Climate Predictions. *NPJ Clim. Atmos. Sci.* **2022**, *5*, 57. [CrossRef]

54. Kug, J.-S.; An, S.-I.; Ham, Y.-G.; Kang, I.-S. Changes in El Niño and La Niña Teleconnections over North Pacific–America in the Global Warming Simulations. *Theor. Appl. Clim.* **2010**, *100*, 275–282. [CrossRef]
55. McGregor, S.; Cassou, C.; Kosaka, Y.; Phillips, A.S. Projected ENSO Teleconnection Changes in CMIP6. *Geophys. Res. Lett.* **2022**, *49*, e2021GL097511. [CrossRef]